JOURNAL OF AIRCRAFT
Vol. 33, No. 3, May–June 1996

Time-Averaged Active Controller for Turbofan Engine Fan Noise Reduction

Russell H. Thomas,* Ricardo A. Burdisso,† and Steven A. Lane‡
Virginia Polytechnic Institute and State University, Blacksburg, Virginia 24061-0238

An active control system has been developed and used experimentally on an operational turbofan engine to reduce inlet tonal noise at the fan blade passage frequency. Both single channel and multichannel systems were tested. The control approach used is the feedforward derivative measurement time-averaged adaptive algorithm. This algorithm is capable of adapting to a nonstationary system, requiring no prior knowledge of the system. A reference sensor mounted in the casing of the fan provides the fan blade passing frequency reference signal to the controller. Microphones with a large sensing area are placed in the acoustic far field of the engine. The control algorithms minimize a cost function, the sum of the error signal mean-square-values, by activating loudspeakers that are mounted around the inlet of the engine. The control signals are obtained by filtering the reference signal with finite impulse response digital filters. The control algorithm finds the optimum filter weights by using statistical estimates of the cost function to be minimized. A single channel control system was tested on an axisymmetric dominant mode case and produced reductions of up to 17 dB at the error microphone. The controller maintained reductions in the fan tone even as the engine speed was increased. In a traverse of the radiated sound field of the engine the fan blade passage tone was reduced over a sector of 30 deg around the error sensor with a considerable spillover increase in the fan tone outside of this sector. Two six-channel control systems were developed and tested on both axisymmetric and spinning mode dominant cases. Reductions of up to 19.7 dB were achieved over large sectors around the error microphones with significantly reduced spillover.

Nomenclature

C = cost function
D = diameter of engine at the fan stage
d = disturbance signal
e = error signal
T = transfer function
u = input signal to control sources
w = adaptive finite impulse response filter coefficients
x = reference signal
y = control source output signal
γ = coherence
μ = convergence parameter

Introduction

THE introduction of ultra high bypass (UHB) ratio turbofan engines in the near future, with bypass ratios from 10 to 15, has put an emphasis on new fan noise reduction technology. This is because the UHB engines will have smaller inlet diameter-to-length ratios and will operate at much lower frequencies then current turbofan engines. These two factors will make it difficult for passive acoustic liner technology to produce additional noise reductions. Several active control methods are being investigated to provide the additional levels of fan noise reduction.

One approach to active fan noise reduction uses a second control noise field to destructively interfere with the engine fan tone to produce a net reduction in the radiated fan tone level. This approach has been investigated on an operational JT15D turbofan engine.[1-3] In these investigations the controller used for the active noise reduction system employed a feedforward filtered-x least-mean-square (FXLMS) time-domain adaptive algorithm.[4,5] While these investigations have demonstrated considerable progress toward reduction of the fan tones over large forward radiated sectors, the FXLMS algorithm has also demonstrated two features that would be desirable to remove. First, the time-domain controller must sample and perform all computations for the control signal update before the next sample, essentially in real time, placing a severe computational speed requirement on the digital signal processor. Second, the filtered-x signal for the time-domain controller requires a system identification, a measurement of the transfer functions between control and error transducers. This system identification is valid for a particular system condition, and if, in the case of an aircraft engine, the engine speed, angle of attack, temperature, etc., were to vary, the system would change and a new identification would need to be carried out. From an application point of view, the elimination of these two features would make the implementation of an active control system more viable.

An alternative control approach to the time-domain FXLMS algorithm is investigated in this work. This control approach uses statistical estimates obtained from time-averaged measurements of the cost function in conjunction with a search algorithm to minimize the error signal power. The control system does not require identification of the control-error path unlike the FXLMS algorithm. These time-averaged (TA) algorithms can differ according to the search method used and two methods were investigated in this work. A single-input single-output (SISO) TA controller with a steepest descent (SD) search algorithm is first described in this work. This algorithm was extended to a six-input six-output (6I6O) SDTA controller. And finally, a pseudo-Newton search algorithm is used with the 6I6O controller to increase the speed and accuracy of the search algorithm.

Received Oct. 24, 1995; revision received Jan. 26, 1996, accepted for publication Jan. 27, 1996.

*Research Scientist, Vibration and Acoustics Laboratories, Mechanical Engineering Department; currently at Virginia Consortium of Engineering and Science Universities, 303 Butler Farm Road, Suite 101, Hampton, VA 23666. Member AIAA.

†Assistant Professor, Vibration and Acoustics Laboratories, Mechanical Engineering Department.

‡Graduate Research Student, Vibration and Acoustics Laboratories, Mechanical Engineering Department.

Adaptive Feedforward Control

The analysis presented here will be carried out in the discrete domain. Thus, a subscript k indicates the signal sample at time t_k. Figure 1 is the general block diagram for an adaptive feedforward controller. The sinusoidal disturbance sequence x_k acts on the plant through the disturbance-error path transfer function $T_{de}(z)$, and generates the response d_k to be minimized. The coherent reference signal, here assumed to be the same disturbance signal x_k, is filtered by an adaptive filter, whose output is the control sequence u_k. For the case of a harmonic disturbance, a two-weight finite impulse response (FIR) filter is sufficient to modify the phase and magnitude of the reference signal. That is, the control sequence is given by

$$u_k = w_0(k)x_k + w_1(k)x_{k-1} \tag{1}$$

where $w_0(k)$ and $w_1(k)$ are the adaptive filter weights, and their dependence with k implies that they are time dependent.

The response of the system because of the control input u_k acting on the control-error path transfer function $T_{ce}(z)$ yields y_k. The error sequence is the superposition of the response because of the sum of the disturbance and control inputs as

$$e_k = d_k + y_k \tag{2}$$

All feedforward control algorithms adjust the FIR filter weights by minimizing a cost function related to the error signal output e_k. The cost function is defined as a mean-squared-value of the error signal given by

$$C(w_0, w_1) = E[e_k^2] \tag{3}$$

where E is the expected value operator. It is straightforward to show that the cost function is quadratic with respect to the filter weights and has only one global minimum.

Time-Domain FXLMS Algorithm

Though the FXLMS algorithm has been described in detail previously,[4,5] a brief description is presented here for comparison with the TA approach as well as for the sake of completeness. The update equation for the FXLMS algorithm is[4,5]

$$\{W\}_{k+1} = \{W\}_k - \mu\{\nabla C_k\} \tag{4}$$

where the μ is the step-size parameter that controls the rate of convergence and the stability of the minimization process, $\{W\}_k = \{w_0(k), w_1(k)\}^T$ is the weight vector; and $\{\nabla C_k\}$ is the instantaneous gradient vector at sample time t_k. Equation (4) shows that the filter weights are updated at each sample period by moving the weights in the direction opposite to the instantaneous gradient vector. The instantaneous gradient vector component is computed by differentiating the instantaneous error signal mean-square-value $(e_k)^2$ with respect to the filter weights. This yields

$$\{\nabla C_k\} = \{2e_k\tilde{x}_k, 2e_k\tilde{x}_{k-1}\}^T \tag{5}$$

where $\tilde{x}$, denoted as the filtered-x signal, is generated by filtering the reference signal x_k by an estimate of the control-error path transfer function. The product $2e_k\tilde{x}_{k-j}$ in Eq. (5) represents the instantaneous jth component of the gradient vector. Thus, the vector in Eq. (5) is not the true gradient of the cost function defined in Eq. (3).

It is clear from Eq. (5) that to implement this algorithm the transfer function $T_{ce}(z)$ needs to be measured, modeled, and used to generate the sequence $\tilde{x}_k$. For the single-frequency case considered here, the transfer function $T_{ce}(z)$ can again be modeled by a two-coefficient FIR filter. However, the two-weight FIR filter will only yield an accurate estimate of the gradient vector $\{\nabla C_k\}$ at the excitation frequency if it remains constant.

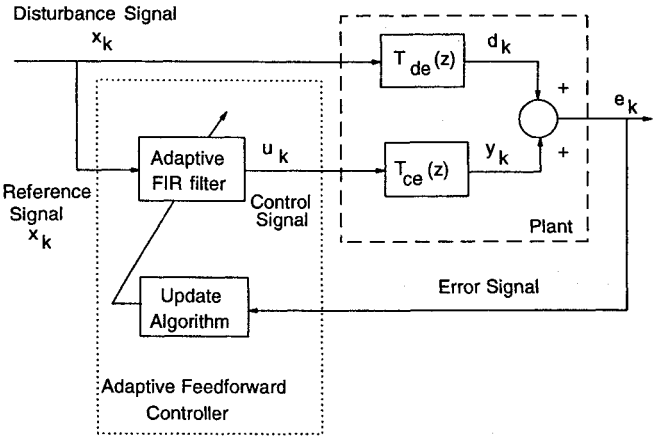

Fig. 1 Block diagram for a general adaptive feedforward controller.

For a varying excitation frequency or complex disturbance input, i.e., multiple frequencies and broadband, the filter modeling $T_{ce}(z)$ should be such that it represents the control-error transfer function over the whole operating frequency range of the disturbance. For these cases, a large-size FIR filter or an infinite impulse response (IIR) filter can be used. However, neither the FIR nor the IIR filter will remain valid if the dynamics of the system changes with time, i.e., varying flow speed, temperature, operating engine conditions, etc. The FXLMS approach has shown some degree of robustness in the event of minor system changes, but significant variations require recalculating $T_{ce}(z)$ for a stable controller.

Two approaches have been proposed to overcome this problem associated with the FXLMS algorithm. The first one is by monitoring continuously $T_{ce}(z)$ using a white noise probe signal uncorrelated to the disturbance input.[6] Using this probe signal the transfer function $T_{ce}(z)$ is modeled in real time. The second approach attempts to simultaneously adapt the weights of both the feedforward compensators and the filter modeling the control-error path transfer functions.[7] This approach was implemented for the case of single frequency excitation of a plate and the results showed some lack of robustness. The drawback of both methods are the increase in the controller complexity and the serious penalty in computational load that can severely reduce the effective controller bandwidth.

Time-Averaged Algorithms

A new update algorithm is proposed here to find the optimum filter weights without having prior knowledge of the control-error path transfer functions. As mentioned before, the cost function is a quadratic function of the filter weights for stationary signals. The main goal of the proposed method is to develop a procedure that efficiently searches the cost function to find the optimum filter weights using only statistical estimates of the cost function. Thus, the proposed approach differs mainly from the previous approaches in that no attempt is made to model the control-error path. The proposed TA update algorithm is illustrated in Fig. 2. The proposed approach consists of minimization cycles. In each cycle, a descent search direction $\{S\}_i$ and a convergence parameter μ_i is first determined. The minimization direction defines a plane that intersects the cost function yielding a parabola. The filter weights are then updated along this direction for a time l consisting of N samples, $l = Nt_s$, where t_s is the sampling period. Thus, the update equation for the ith minimization cycle is given by

$$\{W\}_{l+1} = \{W\}_l + \mu_i\{S\}_i \tag{6}$$

The updating of the filter weights using Eq. (6) is carried out until the cost function is minimized along the one-dimensional search direction $\{S\}_i$. The weight vector that yields the

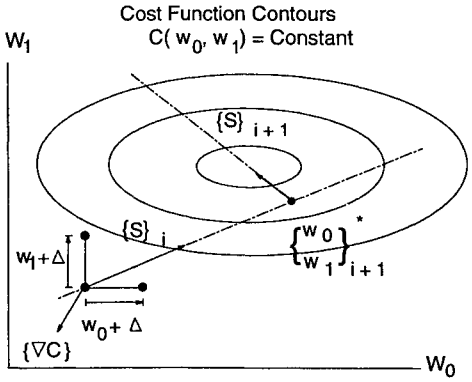

Fig. 2 Time-averaged gradient update approach.

minimum cost function along the $\{S\}_i$ direction is denoted in Fig. 2 as $\{W\}^*_{i+1}$. At this point, a new search direction $\{S\}_{i+1}$ and the convergence parameter μ_{i+1} is determined, and the new minimization cycle is initiated. The one-dimensional minimization cycle continues until the process converges to the optimum weight vector that yields the global minimum. It is clear that the characteristics and the performance of the update algorithm are determined by the selection of the search direction $\{S\}_i$ and the step parameter μ_i. The steepest descent and the Newton's methods are two of the most well-known approaches to search for the minimum of a quadratic cost function in many engineering fields.[8] Based on these methods, two weight update algorithms are proposed here that are denoted as the steepest descent time-averaged (SDTA) and pseudo-Newton time-averaged (PNTA) algorithms, respectively.

SDTA Algorithm

In the SDTA method the search direction is chosen as the negative of the gradient vector

$$\{S\}_i = -\{\nabla C\}_i = -\left\{\frac{\partial C}{\partial w_0}, \frac{\partial C}{\partial w_1}\right\}^T_i \tag{7}$$

where the subscript i indicates that the gradient is computed at $\{W_i\}^*$, which was obtained from the $(i-1)$th minimization cycle. The gradient components in Eq. (7) are computed by evaluating the performance function at two points using a finite difference technique. Thus, for one of the weights

$$\left(\frac{\partial C}{\partial w_0}\right)_i = \frac{C(w_{0i} + \Delta, w_{1i}) - C(w_{0i}, w_{1i})}{\Delta} \tag{8}$$

where Δ is the weight perturbation parameter. This process is also graphically illustrated in Fig. 2. Thus, the update equation becomes

$$\{W\}_{i+1} = \{W\}_i - \mu_i\{\nabla C\}_i \tag{9}$$

where, unlike in the FXLMS algorithm, $\{\nabla C\}_i$ is now the true gradient vector of the cost function to be minimized as defined in Eq. (3). The step size μ_i depends upon the curvature of the parabola defined by $\{S\}_i$. The curvature κ_i can be estimated by evaluating the cost function at three points along the direction $\{S\}_i$. Then, the step size can be estimated at each cycle as follows:

$$\mu_i < 1/2\kappa_i \tag{10}$$

The step size can also be set to a constant value for all possible minimization cycles by a trial-and-error process carried out on the same control system setup.

The main advantage of this algorithm is its simplicity and the few computations involved in the gradient estimation. However, the direction of the negative gradient in general does not point towards the minimum of the cost function, which is its main disadvantage. For a cost function that is significantly distorted, i.e., having an elongated valley, the minimization path can result in a zigzag pattern. This phenomena yields a very slow adaptation process or even failure to converge if the cost functions required in Eq. (8) are not estimated accurately because of noise. This problem can be overcome by a variable transformation.[8] However, this technique requires extensive, previous knowledge of the system, and it is not feasible in this control application.

PNTA Algorithm

In view of the problems associated with the SDTA algorithm, a second approach was developed based on the Newton's method. In the Newton's method, the descent direction is defined as

$$\{S\}_i = -[H]^{-1}\{\nabla C\}_i \tag{11}$$

where $[H]$ is the Hessian matrix given by

$$[H] = \begin{bmatrix} \left(\frac{\partial^2 C}{\partial w_0^2}\right) & \left(\frac{\partial^2 C}{\partial w_0 \partial w_1}\right) \\ \left(\frac{\partial^2 C}{\partial w_1 \partial w_0}\right) & \left(\frac{\partial^2 C}{\partial w_1^2}\right) \end{bmatrix} \tag{12}$$

and the step parameter μ_i is set to unity. Then, the update algorithm becomes

$$\{W\}_{i+1} = \{W\}_i - [H]^{-1}\{\nabla C\}_i \tag{13}$$

The main advantage of this search direction is its quadratic convergence rate. This means that for a quadratic cost function with no noise the convergence is guaranteed in a minimum number of cycles, i.e., two for the case considered here. This approach also removes the need for guessing a step size, since it is defined as one.

However, this update algorithm presents serious implementation difficulties. Firstly, the numerical computation of the second derivatives is generally more involved than the first derivative in Eq. (8). Secondly, the number of second derivatives to compute increases with the square of the number of adaptive weights to update, which will be discussed later. Thirdly, the main drawback in implementing Eq. (13) is the need to compute the inverse of the Hessian matrix. Since the numerical estimation of the second derivatives will always contain some degree of error, i.e., because of noise in the signal, the inverse of matrix $[H]$ could yield erroneous results.[9] Matrix $[H]$ could also be singular, in which case the inverse would not exist. All of these problems are more serious for the implementation of multiple-input multiple-output (MIMO) systems as it will be pointed out later.

To overcome these drawbacks and still take advantage of the positive features of this method, a modified update equation is proposed, referred to here as the pseudo-Newton method. The update equation is

$$\{W\}_{i+1} = \{W\}_i - \mu_i[\hat{H}]^{-1}\{\nabla C\}_i \tag{14}$$

where matrix $[\hat{H}]$ consists of only the diagonal elements of the Hessian matrix $[H]$. The assumption in this approximation is that the off-diagonal elements are negligible for a quadratic cost function. The numerical computation of the elements in matrix $[\hat{H}]$ is accomplished by perturbing the weight twice. For example, the second derivative for w_0 is

$$\frac{\partial^2 C}{\partial w_0^2} = \frac{C(w_0 + \Delta, w_1) + C(w_0 - \Delta, w_1) - 2C(w_0, w_1)}{\Delta^2} \tag{15}$$

The pseudo-Newton method in Eq. (14) has several advantages over the Newton's method in Eq. (13). Firstly, the number of numerical approximations for the second derivatives is equal to the number of filter weights, greatly reducing the computations. Secondly, the inversion of the Hessian approximation is trivial. Thirdly, since the updating process in Eq. (14) takes into consideration the curvature of the performance surface through the Hessian approximation, the step size can again be set to $\mu_i \leq 1$ as in the pure Newton's method. In this approach, the parameter μ_i is estimated based on the norm of the gradient vector $\|\nabla C_i\|$, computed at the initial point of each minimization cycle. This factor is defined as

$$\mu_i = 1 - [1/(1 + \|\nabla C_i\|)] \tag{16}$$

Even though a $\mu = 1$ would yield a stable controller, the step-size factor was introduced to further increase the stability and as an added measure of safety, yielding a more robust controller, tolerant of noise in the system. Near the optimum filter weights, the norm of the gradient vector will approach zero and $\mu_i \to 0$. On the other hand, away from the optimum filter weights, the norm of the gradient vector will be larger than unity and $\mu_i \to 1$. Thus, this step-size scaling eliminates meandering of the filter weights near their optimum values.

Multi-Channel Control System

The simple case of a SISO control system presented in the previous section was used to introduce the proposed control algorithms. However, a realistic control system will consist of a multichannel system.[10] In this section, the application of the control approaches to multichannel systems is discussed.

A multichannel control system is illustrated in Fig. 3. The system has N_c control inputs u_{ik} ($i = 1, \ldots, N_c$), and the response of the system is monitored by N_e error sensors whose outputs are the error signals e_{jk} ($j = 1, \ldots, N_e$). The control signals are generated by feeding forward the same reference signal to N_c adaptive two-weight FIR filters. The update algorithm will have to adjust the coefficients of the FIR filters to minimize a cost function related to the N_e error outputs. The cost function to be minimized is now the sum of the error signal mean-square-values. That is,

$$C(w_{01}, w_{11}, w_{02}, w_{12}, \ldots) = \sum_{j=1}^{N_e} E[(e_j)_k^2] \tag{17}$$

It is straightforward to show that the cost function in Eq. (17) is again a quadratic function of the adaptive filter weights. Thus, the update algorithms developed for the SISO case can be readily expanded to the MIMO control system. This is accomplished by grouping the filter weights on a single vector as

$$\{W\} = \{\mathbf{w}_{01}, \mathbf{w}_{11}, \mathbf{w}_{02}, \mathbf{w}_{12}, \ldots, \mathbf{w}_{0N_c}, \mathbf{w}_{1N_c}\}^T \tag{18}$$

and replacing it into the update equation in Eq. (6). The search direction will be

$$\{S\}_i = -\left\{\frac{\partial C}{\partial w_{01}}, \frac{\partial C}{\partial w_{11}}, \frac{\partial C}{\partial w_{02}}, \frac{\partial C}{\partial w_{12}} \cdots\right\}_i^T \tag{19}$$

for the SDTA method, and for the PNTA approach

$$\{S\}_i = -\begin{bmatrix} \left(\frac{\partial^2 C}{\partial w_{01}^2}\right)^{-1} & & & \\ & \left(\frac{\partial^2 C}{\partial w_{11}^2}\right)^{-1} & & \\ & & \ddots & \\ & & & \left(\frac{\partial^2 C}{\partial w_{1N_c}^2}\right)^{-1} \end{bmatrix} \begin{Bmatrix} \frac{\partial C}{\partial w_{01}} \\ \frac{\partial C}{\partial w_{11}} \\ \vdots \\ \frac{\partial C}{\partial w_{1N_c}} \end{Bmatrix} \tag{20}$$

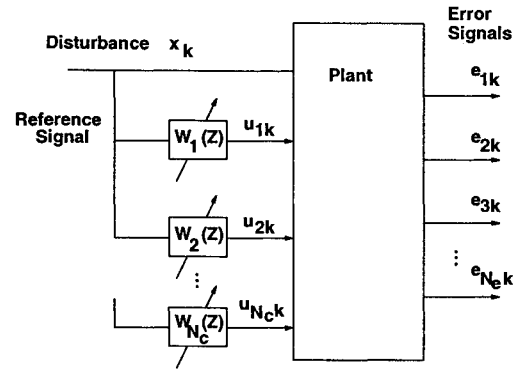

Fig. 3 MIMO feedforward control system.

The advantages of using the pseudo-Newton approach in Eq. (15) rather than the pure Newton's method in Eq. (14), for MIMO control systems is now clear. The pseudo-Newton approach requires to compute $2N_e$ second derivatives and the inversion of $[\hat{H}]$ is trivial. In contrast, the Newton's approach requires $N_c(2N_c + 1)$ second derivatives computations and the inversion of a $2N_c \times 2N_c$ matrix.

For comparison purposes, in the FXLMS MIMO controller, the final form of the FIR coefficient update equation is given by[10]

$$w_{sj}(k + 1) = w_{sj}(k) - 2\mu \sum_{i=1}^{N_c} (e_i)_k (\bar{x}_{ji})_{k-s}$$

$$s = 0, 1 \quad j = 0, 1, \ldots, N_c \tag{21}$$

where $w_{sj}(k)$ represents the sth coefficient of the jth adaptive filter, $(\bar{x}_{ji})_k$ is defined as the reference signal filtered by the transfer function between the jth control input and the ith error sensor; $s = 0, 1; j = 1, \ldots, N_c$; and N_c and N_e are the number of control and error channels, respectively. For a MIMO control system, Eq. (21) shows that $N_e \times N_c$ transfer functions need to be measured, and used to predict an equal number of filtered-x signals. In addition, the step parameter μ that will yield a stable adaptation process is inversely proportional to the sum of the filtered-x signal power. It is clear that increasing the number of control channels will quickly reduce both the effective bandwidth of the multichannel controller and the convergence rate.

Experimental Apparatus and Method

The approach is to experimentally implement an adaptive feedforward active noise control system on an operational turbofan engine. The system reduces the level of a tone produced by the engine by the destructive interference of a control and disturbance sound fields. The active control system has four main components. A reference sensor provides a coherent signal with information on the frequency of the disturbance tone; this signal is fed forward to the adaptive filters that generate the control signals. Error sensors are placed in the acoustic far field of the engine to measure the resultant noise. A schematic of the engine, test cell, and the components of the controller are shown in Fig. 4 and will be discussed later. In Fig. 4, a SISO controller is shown for simplicity.

Engine and Test Cell

A Pratt and Whitney JT15D-1 turbofan engine is mounted in a test cell at Virginia Tech. It is a twin-spool turbofan engine with a bypass ratio of 2.7. It has a single-stage axial flow fan with 28 blades and a centrifugal high-pressure compressor with 16 full vanes and 16 splitter vanes. There are no inlet guide vanes. The maximum rotational speed of the low-pressure

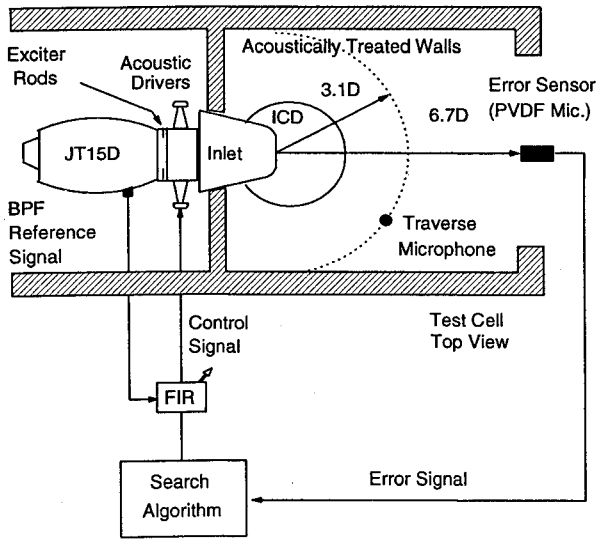

Fig. 4 Turbofan engine, test cell, and active control system experimental apparatus.

spool is 16,000 and 32,760 rpm for the high-pressure spool. The fan has a pressure ratio of 1.5 and a hub-to-tip ratio of 0.41. The low-pressure stator assembly following the fan consists of an outer stator in the bypass duct that has 66 vanes and 71 vanes in the core stator assembly. The acoustics of this particular engine have been substantially studied and reported.[11-13]

The engine is equipped with an inlet control device (ICD) mounted on the inlet. This ICD was built at Virginia Tech using a NASA design.[14] The purpose of the ICD is to minimize the spurious effects of ground testing on acoustic measurements. The engine is mounted in a test cell that is divided by a wall so that the forward section of the test cell is a semianechoic chamber where only the inlet of the engine is inside the chamber. The walls of the semianechoic chamber are covered with 7.6-cm-thick acoustic foam that minimizes reverberations and minimizes the influence of the noise from the jet of the engine.

Active Control Apparatus

Either 27 or 28 exciter rods, 0.48 cm in diameter and equally spaced circumferentially, were placed $0.19D$ upstream of the fan stage. These rods extend 27% of the length of the fan blades through the outer casing into the flow. The wakes from the rods interact with the fan blades producing tones that are significantly higher in sound level than those produced without the interactions. The purpose of the rods is to produce a specific acoustic mode. With 28 rods, a number equal to the 28 fan blades, a plane wave mode is produced although higher-order radial modes are also generated.[15] The plane wave mode has a uniform pressure amplitude over the inlet cross section and propagates at all frequencies beaming along the engine axis.[16] With 27 rods, the first-order circumferential spinning modes are generated and the radiation directivity pattern of that mode has a notch along the engine centerline.

The forward-radiated engine noise spectrum is marked by three significant tones in the audible range, the fan blade passage frequency (BPF) tone at about 2360 Hz, the 2 BPF tone at about 4720 Hz, and the high-pressure BPF tone at about 4100 Hz. These approximate frequencies correspond to the idle operating condition of the engine with the low-pressure spool at 31% of full speed and the high-pressure spool at 46% of full speed. The engine was run at idle condition so that these three tones would be in the audible range and, for the frequencies involved, all three tones would be within the computational speed requirements of the controller.

The reference signal that is required by the controller is produced by a sensor mounted flush with the casing of the fan. This eddy-current sensor picks up the passage of each fan blade and provides a very accurate time history measure of the fan BPF.

The loudspeakers attached to the circumference of the inlet are the control sound sources. They are actuated by the controller producing the control field. Two loudspeakers are attached to each horn for a total of 12 horns and 24 loudspeakers. The loudspeakers are commercially available 8-Ω drivers capable of 100 W on a continuous program with a flat frequency response to within 2 dB from 2 to 5 kHz. The horns have a throat diameter of 1.9 cm with an exponential flare in the direction of flow in the inlet. The horn opening in the inlet wall is 1.9 $\times$ 7.6 cm.

Error sensors are the last component of the active control hardware. They measure the resultant noise of the engine and control sound sources. The engine sound radiation pattern is characterized by the presence of lobes and notches and can be unsteady. The placement of point error microphones near these lobes results in an unsteady error signal. To overcome this problem, a large area transducer was devised that spatially averages the incident sound pressure.[1,3] These error sensors were made of a polyvinyldine-fluoride (PVDF) film 7.6 cm in diameter. These large-area PVDF microphones are uncalibrated and produce a relative measurement of sound pressure level.

Experimental Results

SISO Control of the Plane Wave Mode

Twenty-eight exciter rods were installed to produce the plane wave and higher-order axisymmetric radial modes dominant mode. A SISO SDTA controller was used to control the radiated sound at the fan BPF tone, at 2325 Hz for this specific experiment. One PVDF error microphone was placed at a distance of 6.7 fan diameters from the inlet lip of the engine, directly on the centerline. The PVDF error microphone is both highpass and lowpass filtered so that the fan BPF tone is the dominant signal. The peak level of the fan BPF tone is 81.7 dB at 2325 Hz, recalling that this is not a calibrated absolute sound pressure level. The control algorithm usually takes between 10-30 s to converge and reduce the fan BPF tone level by up to 17 dB.

The traverse microphone is a high-quality microphone calibrated for absolute measurement of sound pressure level (SPL) (dB referenced to 20 μPa) and was placed on the engine axis at a distance of 3.1 fan diameters. The controlled level of the fan BPF tone was 11.9 dB lower than the uncontrolled level at the error microphone location. A radiation directivity plot is obtained when the traverse is swept from +90 to −90 deg around the engine inlet and the uncontrolled and controlled levels are measured at each location (Fig. 5). A region of reduced SPL extends for 15 deg around the centerline location of the PVDF error microphone. Beyond this region the controlled levels are actually higher than the uncontrolled levels. The control system is minimizing the error signal only, without any error sensors in the off-axis region there is no effort to reduce the tone levels in this region. Previous work[2,3] has demonstrated, with the FXLMS controller, that increasing the number of control channels increases the area in which the radiated sound field can be reduced. However, the control actuators must be coupled to the inlet acoustics in such a way that the far-field directivities of the engine and the control actuators match. The engine has a directivity that is strongly beamed forward. This can be seen from the directivity labeled controlled in Fig. 5 that, even though it is the directivity of the control field with the engine on, is indicative of the directivity produced by the control sound sources alone. As noted in Fig. 5, the directivity of the control sound sources is more uniform. The control sources must match the high levels of the engine on the axis where the error microphone is placed resulting in the significant levels of spillover off-axis.

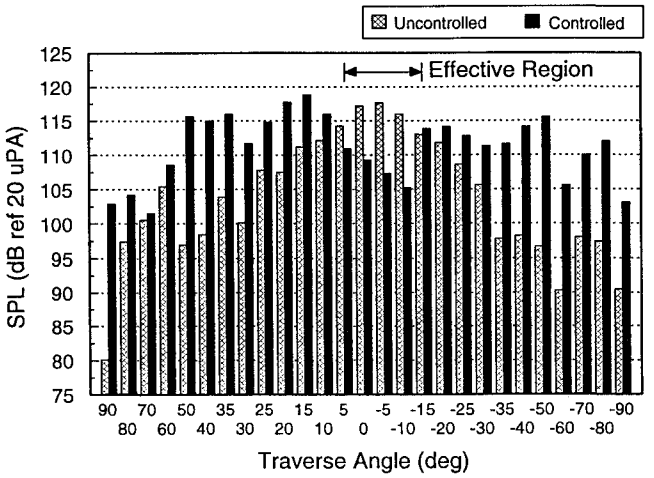

Fig. 5 Radiation directivity of the axisymmetric case controlled by a SDTA SISO controller, fan BPF tone at 2325 Hz. Engine centerline at 0 deg.

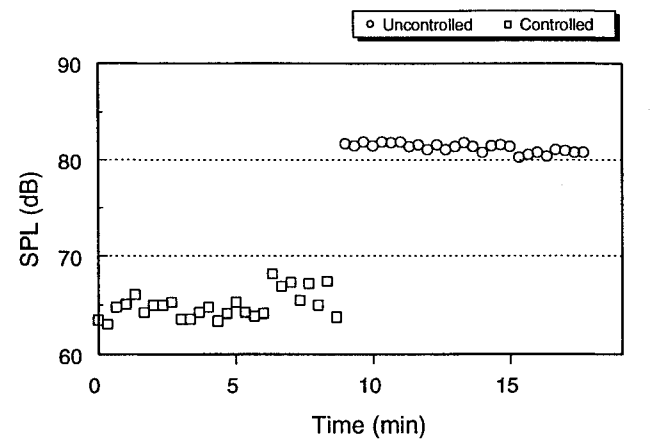

Fig. 6 Time history of the fan BPF tone level recorded by the error microphone with and without control, SDTA controller used on the axisymmetric mode case.

With the engine at a constant speed, a spectrum of the error microphone is recorded to intervals of 20 s and the fan BPF tone level time history is obtained with and without control as shown in Fig. 6. For the first 9 min the controller maintains control of the fan BPF tone. The controller is turned off and the fan BPF tone level returns to the uncontrolled level. This demonstrates the robustness of the controller to maintain control of the fan BPF tone over long periods of time.

SISO Control with Engine Speed Change

In the process of updating the gradient estimations, the controller is measuring the system response to the perturbations in the filter weights. In this way, the controller can take into account the effect of any change in the system with the measurement of the cost function. These changes can include angle of attack of the engine or atmospheric changes in pressure and temperature or, more likely, a change in the engine speed. As the speed of the engine increases and the fan BPF increases, the controller will update the coefficients with new system information included and maintain control (Fig. 7). The control of both the traverse microphone and the error microphone are measured over a change in fan BPF of almost 150 Hz.

In previous work[1-3] where the FXLMS controller was used, a system identification is required to provide the filtered-x signal. The system identification was a measurement of the transfer function from the controller to error microphone. This transfer function was modeled for only one operational engine condition, this identification is valid only for one engine speed.

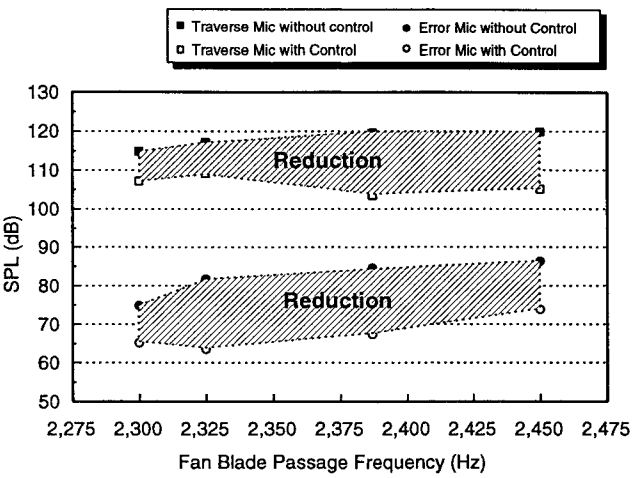

Fig. 7 SDTA algorithm control of the fan BPF tone with change in engine speed.

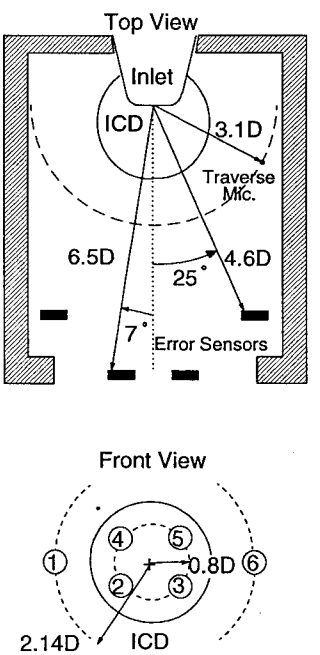

Fig. 8 Far-field error sensor locations for axisymmetric mode control using 6I6O SDTA controller. Dimensions in terms of fan diameter *D*.

Change in the engine speed while maintaining control of a tone is not possible with the time-domain controller unless the transfer function is valid for a range of operational conditions. The ability of the TA controller to adapt to system changes and maintain control is a significant improvement over the FXLMS approach. This system adaptive capability is crucial to eventual application.

6I6O Control of the Axisymmetric Mode

To minimize the off-axis spillover and increase global reduction of the fan BPF tone a six-channel (6I6O) control system was developed and tested. The output from the six adaptive filters generate the control signals that drive the control sources, which consist of the 12 sets of loudspeakers. Each control signal drives a pair of these loudspeakers, with each loudspeaker of the pair opposite to the other across the inlet duct. For the case with the axisymmetric mode dominant, the six far-field PVDF error sensors were located as in Fig. 8. Distances to the error microphones are measured from the inlet of the engine. The SDTA algorithm was used to reduce the error signals at the fan BPF tone. The levels of reduction for

Table 1 Error microphone reductions achieved with six-channel controllers on axisymmetric and spinning mode cases[a]

	Error signal reduction, dB					
Experiment controller	1	2	3	4	5	6
Axisymmetric mode case						
SDTA[b]	10.2	3.4	3.2	3.0	2.8	10.2
Spinning mode case						
SDTA[c]	19.7	13.7	5.7	17.2	8.8	4.4
PNTA[c]	17.2	11.4	6.4	7.0	15.9	5.8

[a]The error sensor locations are different for the three experiments listed.
[b]Figures 8 and 9.
[c]Figures 10 and 11.

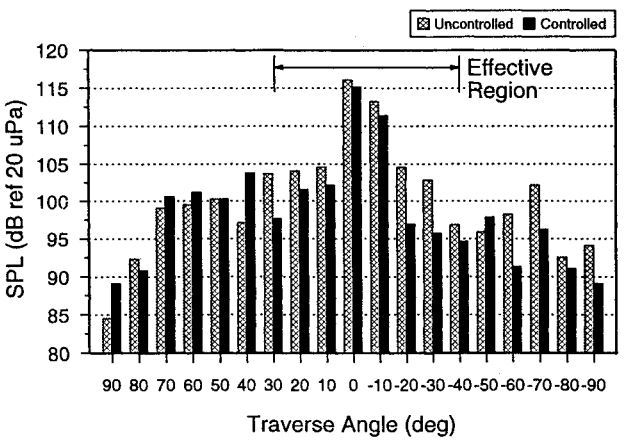

Fig. 9 Radiation directivity for the 6I6O SDTA controller on the axisymmetric mode case, for a fan BPF of 2475 Hz.

the six microphones are shown in Table 1. The radiation directivity is shown in Fig. 9, which shows far-field reduction over a sector from +30 to −40 deg with a minimal amount of spillover toward the sideline from +50 to +90 deg and reduction toward the other sideline from −60 to −90 deg.

6I6O SDTA and PNTA Control of the Spinning Mode

The 6I6O set of experiments were carried out to control the first-order circumferential spinning modes (1,0), (1,1), and (1,2) produced by inserting 27 rods upstream of the 28 fan blades. The control actuator arrangement for the 6I6O axisymmetric mode case would produce high levels on the centerline. However, the first-order spinning mode produces a notch in the radiation directivity at the centerline 15 dB lower than the peak levels found at 15–20 deg off of the centerline.

Therefore, the loudspeakers within each pair were wired 180-deg out-of-phase. This way each channel of control consisting of two loudspeakers, each opposite the other across the inlet, would produce a notch at the centerline and be able to match the directivity of the spinning mode. The error sensor placement is shown in Fig. 10 for the experiment using the SDTA controller. The PNTA controller was tested with an error configuration similar to that in Fig. 8, except that the center four microphones were still 0.8D off the centerline, but closer in distance from the inlet at 4.29D, making them 10 deg off of the centerline, and the two outside microphones were still at 25 deg but were closer at 3.81D. This slight change in error microphone placement was because of the PNTA experiment done at a slightly different BPF, which alters the directivity slightly. Table 1 also summarizes the results for the two experiments in terms of the reduction achieved at the six error microphones.

The reduction at the six error microphones are comparable for the two algorithms. The radiation directivity of the SDTA controller is shown in Fig. 11. Figure 11 shows reduction at ±20 and ±30 deg with some reduction toward the sideline areas. The PNTA algorithm experiment showed less reduction

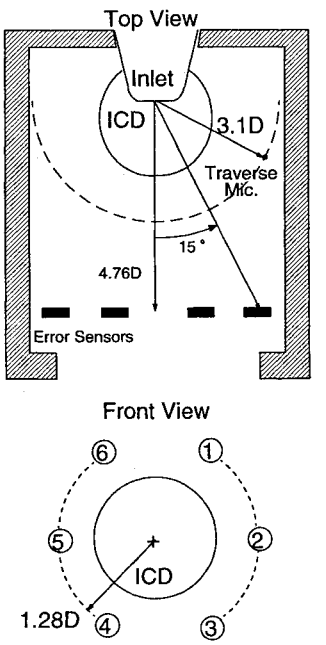

Fig. 10 Error sensor placement for control of the spinning mode with the 6I6O SDTA controller.

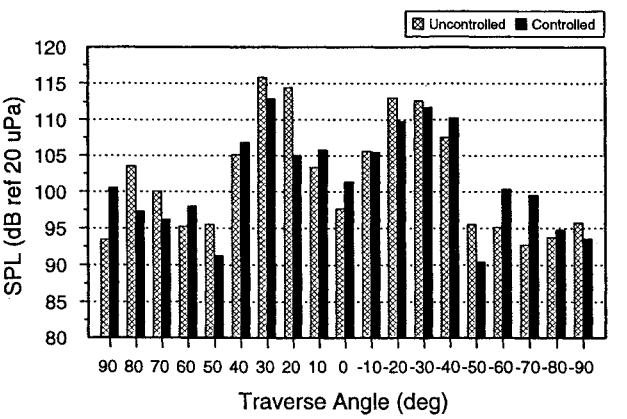

Fig. 11 Radiation directivity plot for the 6I6O SDTA controller, spinning mode experiment, with fan BPF tone at 2500 Hz.

in the ±20- to ±30-deg areas, but still some reduction toward the sideline areas. In general, using the SDTA or the PNTA algorithm produced similar results in the far field. It is important to note that this was not an exhaustive, detailed comparison, but rather was meant to indicate a general result. Very importantly, all three 6I6O experiments (Figs. 9 and 11) and the PNTA algorithm showed minimal spillover as compared to the SISO experiment. This does indicate that increasing the degrees of freedom of the controller by increasing the number of channels does give the controller more flexibility to match the directivity of the engine. More improvement can be made

with better coupling of the control actuators with the duct acoustics by having, for example, multiple axial locations of control actuators.

Conclusions

A time-averaged control algorithm was developed for an active control system for the reduction of turbofan engine fan tones. This time-averaged approach differs from the previously used filtered-x approach primarily in that the system identification is done implicit in the time-averaged measurements of the system, and therefore a separate system identification procedure, required by the FXLMS approach, is not required. The computational structure that results for the two approaches results in significant differences in their capabilities. The FXLMS approach performs all computations in real time. The time-average algorithm shifts a large fraction of the computations off-line, which increases the maximum bandwidth of the controller. This becomes particularly important as the number of channels of control increases. The primary advantage of the time-averaged controller is its ability to adapt to changes in the system such as angle of attack, temperature, flow speed, etc. This feature is a key to eventual application to aircraft turbofan engine noise reduction.

Acknowledgments

This research was sponsored by the Acoustic Systems Technology Group of General Electric Aircraft Engine with Karen Kontos, Robert Kraft, and Philip Gliebe as Technical Monitors.

References

[1]Thomas, R. H., Burdisso, R. A., Fuller, C. R., and O'Brien, W. F., "Preliminary Experiments on Active Control of Fan Noise from a JT15D Turbofan Engine," *Journal of Sound and Vibration*, Vol. 161, No. 3, 1993, pp. 532–537.

[2]Thomas, R. H., Burdisso, R. A., Fuller, C. R., and O'Brien, W. F., "Active Control of Fan Noise from a Turbofan Engine," *AIAA Journal*, Vol. 32, No. 1, 1994, pp. 23–30.

[3]Burdisso, R. A., Thomas, R. H., Fuller, C. R., and O'Brien, W. F., "Active Control of Spinning Acoustic Modes from a Turbofan Engine," AIAA Paper 94-0361, Jan. 1994.

[4]Widrow, B., and Stearns, S. D., *Adaptive Signal Processing*, Prentice–Hall, Englewood Cliffs, NJ, 1985.

[5]Widrow, B., Glover, J. R., McCool, J. M., Kaunitz, J., Williams, C. S., Hearn, R. H., Zeidler, J. R., Dong, E., and Goodlin, R. C., "Adaptive Noise Canceling: Principles and Applications," *Proceedings of the IEEE*, Vol. 63, No. 12, 1975, pp. 1692–1716.

[6]Eriksson, L. J., Allie, M. C., Bremigan, C. D., and Gilbert, T. A., "Active Noise Control on Systems with Time-Varying Sources and Parameters," *Sound and Vibration Magazine*, July 1989, pp. 16–21.

[7]Sommerfeldt, S. D., "Multi-Channel Adaptive Control of Structural Vibration," *Noise Control Engineering Journal*, Vol. 37, No. 2, 1992, pp. 77–89.

[8]Haftka, R. T., and Kamat, M. P., *Elements of Structural Optimization*, Martinus–Nijhoff, Dordrecht, The Netherlands, 1985.

[9]Atkinson, K. E., *An Introduction to Numerical Analysis*, Wiley, New York, 1989, pp. 17–28.

[10]Elliot, S. J., Stothers, I. M., and Nelson, P. A., "A Multiple Error LMS Algorithm and Its Application to the Active Control of Sound and Vibration," *IEEE Transactions on Acoustics, Speech and Signal Processing*, Vol. ASSP-350, No. 10, 1987, pp. 1423–1434.

[11]Preisser, J. S., Schoenster, J. A., Golub, R. A., and Horne, C., "Unsteady Fan Blade Pressure and Acoustic Radiation from a JT15D-1 Turbofan Engine at Simulated Forward Speed," AIAA Paper 81-0096, Jan. 1981.

[12]Preisser, J. S., and Chestnutt, D., "Flight Effects on Fan Noise with Static and Wind-Tunnel Comparisons," *Journal of Aircraft*, Vol. 21, No. 7, 1984, pp. 453–461.

[13]Joppa, P. D., "Acoustic Mode Measurements in the Inlet of a Turbofan Engine," *Journal of Aircraft*, Vol. 24, No. 9, 1987, pp. 587–593.

[14]Homyak, L., McArdle, J. G., and Heidelberg, L. J., "A Compact Inflow Control Device for Simulating Flight Fan Noise," AIAA Paper 83-0680, April 1983.

[15]Tyler, J. M., and Sofrin, T. G., "Axial Flow Compressor Noise Studies," *Society of Automotive Engineers Transactions*, Vol. 70, 1962, pp. 309–332.

[16]Heidmann, M. F., Saule, A. V., and McArdle, J. G., "Analysis of Radiation Patterns of Interaction Tones Generated by Inlet Rods in the JT15D Engine," AIAA Paper 79-0581, March 1979.